Preparation and Characterization of Poly (Lactic Acid) Based Composites Reinforced with Poly Dimethyl Siloxane/ Ultrasound Treated Oil Palm Empty Fruit Bunch

ARTICLE *in* POLYMER-PLASTICS TECHNOLOGY AND ENGINEERING · JANUARY 2015

Impact Factor: 1.48 · DOI: 10.1080/03602559.2015.1010219

5 AUTHORS, INCLUDING:

John Olabode Akindoyo
Universiti Malaysia Pahang
10 PUBLICATIONS **0** CITATIONS
SEE PROFILE

H. Beg
Universiti Malaysia Pahang
98 PUBLICATIONS **641** CITATIONS
SEE PROFILE

Muhammad Remanul Islam
Universiti Malaysia Pahang
23 PUBLICATIONS **76** CITATIONS
SEE PROFILE

Dr. Abdullah Al-Mamun
Hp Pelzer Holding groups, Witten
27 PUBLICATIONS **432** CITATIONS
SEE PROFILE

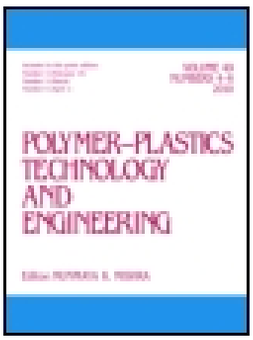

Polymer-Plastics Technology and Engineering

ISSN: 0360-2559 (Print) 1525-6111 (Online) Journal homepage: http://www.tandfonline.com/loi/lpte20

Preparation and Characterization of Poly (Lactic Acid) Based Composites Reinforced with Poly Dimethyl Siloxane/ Ultrasound Treated Oil Palm Empty Fruit Bunch

J. O. Akindoyo, M. D. H. Beg, S. Ghazali, M. R. Islam & A. A. Mamun

To cite this article: J. O. Akindoyo, M. D. H. Beg, S. Ghazali, M. R. Islam & A. A. Mamun (2015): Preparation and Characterization of Poly (Lactic Acid) Based Composites Reinforced with Poly Dimethyl Siloxane/ Ultrasound Treated Oil Palm Empty Fruit Bunch, Polymer-Plastics Technology and Engineering, DOI: 10.1080/03602559.2015.1010219

To link to this article: http://dx.doi.org/10.1080/03602559.2015.1010219

Accepted online: 02 Oct 2015.

PREPARATION AND CHARACTERIZATION OF POLY (LACTIC ACID) BASED COMPOSITES REINFORCED WITH POLY DIMETHYL SILOXANE/ ULTRASOUND TREATED OIL PALM EMPTY FRUIT BUNCH

J. O. Akindoyo, M. D. H. Beg[1], S. Ghazali, M. R. Islam, A. A. Mamun[1]

[1]Institute of Material Engineering, University of Kassel Mönchebergstrasse, Kassel, Germany,[2]Faculty of Chemical and Natural Resources Engineering, Universiti Malaysia Pahang, Kuantan, Malaysia

Mohammad Dalour Hossen Beg, Associate Professor, Faculty of Chemical and Natural Resources Engineering, Universiti Malaysia, Pahang, Malaysia.
E-mail: dhbeg@yahoo.com

Abstract

Oil palm empty fruit bunch (EFB) fiber and poly lactic acid was used to produce composites by melting cast method. Fiber loading was considered up to 40 wt%. EFB fibers were treated using ultrasound and polydimethylsiloxane (PDMS) to improve the interfacial adhesion. The structure and surface properties of the fibers were analysed by Fourier transform of infrared spectroscopy (FTIR), X-Ray diffraction (XRD), scanning electron microscopy and contact angle (CA) measurement. Moreover, FTIR, tensile, flexural, XRD, CA, differential scanning calorimetry and thermogravimetric analysis were used to investigate composites' properties. Analysis revealed that PDMS treatment composites show reduced wettability with increased crystallinity.

KEYWORDS: Poly (lactic acid), biomaterials, compounding, fibers, thermal properties

1. INTRODUCTION

Emergence of polymers in the 19th century ushered in a new era of research with a new option of using the natural fibers in more sophisticated applications. At that time also, there were great interests in synthetic fibers, because of its superior dimension and other properties, which makes it to fit into different applications. However, changes in the raw material and production of synthetic composites required a large quantum of energy and quality of environment suffered because of the pollution generated during the production and recycling of these synthetic materials. This once again drew attention towards natural fibers due to their distinct advantages [1, 2]. The renewed interest in the natural fibers led to a large number of modifications to bring it at par and where possible superior to synthetic fibers and owing to those tremendous changes in the quality of natural fibers [3, 4], they are fast emerging as a reinforcing material in composites [5-8].

Natural fibers are found to have extensive applications in building and civil engineering fields [3]. Moreover, natural fiber based composites are environmentally friendly to a large extent, although the hydrophilic character of natural fibers would lead to composites with weak interface. Also, other challenges associated with natural fiber reinforced composites which makes it less attractive is the inherent low melting point, and poor resistance towards moisture [9, 10]. However, pre-treatments in the form of surface modification could help to improve the adhesion between fibers and matrix, as well as improve other properties. Pre-treatments of natural fibers are aimed at activating the hydroxyl groups or to add new moieties to the fiber surface which can effectively interlock with the matrix. Pre-treatments of the natural fiber can clean the fiber surface,

chemically modify the surface, stop the moisture absorption process, and increase the surface roughness [9-11].

In recent years, natural fiber reinforced composites have received much attention because of their light weight, nonabrasive, combustible, nontoxic, low cost and biodegradable properties. Among the various natural fibers, flax, bamboo, sisal, hemp, ramie, jute, oil palm and wood fibers are of particular interest. Some of the different surface treatment methods that have been applied onto the fiber surface to improve its strength, size, its shape and the fiber-matrix adhesion include alkali treatment [12], silane [13], isocyanate treatment [14], acrylation [8], benzoylation [15], latex coating [16], permanganate treatment [17], and peroxide treatment [1]. However, the combination of alkali and silane treatment of natural fibers had been reported to produce composites with highly desirable properties [8].

Alkali treatment otherwise called mercerization is one of the most commonly used methods for fiber surface modification, especially when the fiber is to be used as reinforcement for either thermoplastics or thermosets. The alkaline treatment removes considerable amount of lignin, hemicelluloses and waxes from the external surface of the fiber cell wall. It also leads to disruption of the hydrogen bonding in the fiber structural framework, leading to an increased surface roughness. It should however be noted that excessive use of alkaline for fiber surface treatment can lead to the removal of excess lignin, which might weaken and damage the fiber [1,18]. The chemical treatment of natural fibers, however, is sometime considered as non-environmentally friendly and

costly. Hence, environmentally friendly and easy method needs to be searched for, for example, ultrasound treatment [19]. This technique involved sound frequency in liquid media, which develop bubbles by a physical process. The sudden coloups of those bubbles may cause high temperature and high presuure shock waves that are adequate to break the chemical bonds [20]. Thorugh tis tecknique, fibers were treated and reported properties of the composites were found to be motivational. On the other hand, silane most often is used as coupling agents to enhance the adherence of fibers to the polymer matrix. They tend to contribute hydrophobic properties to the surface of the fiber through reduction of cellulose hydroxyl groups, thereby reducing its hydrophilicity. Silane treated natural fiber composite provides high tensile strength properties when compared to alkaline treatment [21].

In another vein, the matrix plays a less significant role in the entire tensile load-carrying capacity of the composite material. It should however be noted that its selection has a highly important influence on the compressive, interlaminar shear and also the in-plane shear properties of the resulting polymer composite. Hence the matrix should be compatible with the fiber, both thermally and chemically, and should also be compatible with available fabrication methods for manufacturing the desired composite material [22]. Most of the features such as surface appearance, shape, tolerance to environmental conditions as well as durability all depends on the matrix material while the reinforcement materials are mainly responsible for bearing the structural load thereby providing strength and stiffness of the composite material.

Recently, poly (lactic acid) (PLA) had become an important matrix for polymer composites because PLA is suitable for processing on a large scale industrial production line like injection molding, extrusion, thermoforming and blow moulding at temperatures below its degradation temperature [7, 8, 23]. Thermal degradation of PLA occurs at temperatures above 200^0C. It is therefore necessary to process PLA below this temperature so as to retain its molecular weight and thermal properties. Also, PLA is a thermoplastic with high strength, modulus and which can be obtained from sources that are renewable on an annual basis. It can be fashioned into articles that are used for domestic, industrial packages as well as in the field of medicine. PLA processing is often carried out on standard plastic equipment, to obtain molded parts, fibers or films [24].

In this study, composites were prepared from oil palm empty fruit bunch fiber (EFB) and PLA. The fibers were treated with ultrasound in an alkali medium and later treated with silane or poly(dimethylsiloxane) (PDMS) and the effect of treatment on fiber as well as composite properties were investigated and reported herein.

2 Materials And Method

2.1 Materials

PLA (of Natureworks Ingeo^{TM} Biopolymer 3051D grades) with density of 1.24 g/cm^3, melt flow index of 30-40g / 10 min (190^{o}C/2.16kg) and a melting temperature of 160-170^{o}C, was purchased from Unic Technology Ltd, China. The EFB fibers were collected from LKPP Corporation Sdn. Bhd., Kuantan, Malaysia. Sodium hydroxide, acetic acid

and acetone were procured from Merck, Germany. PDMS was procured from Sigma Aldrich, USA.

2.2. Methods

2.2.1. Fiber Content Optimization

Raw EFB fibers contained several dirt particles ranging from sands, seed grains, seed shells, palm fruits, palm seeds and mud. These were removed by washing the EFB fibers in continuous water flow after which they were dried in air for 24 h. Dried fibers were cut into random short sizes of about 2-5 mm. For composites fabrication, EFB fibers (10, 20, 30 and 40 wt% content) were compounded with PLA using a twin screw extruder (Thermo Scientific Prism Eurolab-16, Germany) fitted with a fixed length pelletizer. Samples were prepared for testing from dried pellets (70^{o}C for overnight) using an injection moulding machine (model- DR BOY 22M). Processing parameters for extrusion and injection moulding are put together in Table 1. The best performances in mechanical properties were obtained from composites with 30 wt% EFB fiber content. This was regarded as the optimum fiber content for this research.

2.2.2. Fiber Treatment And Composite Fabrication

Treatment of EFB fibers was carried out in a two stage process. Firstly, ultrasound treatment in an alkali medium (2% NaOH) (fiber to water ratio of 1:20 at 90^{o}C for 100 min) was conducted to the fibers in order to activate the –OH of EFB fiber cellulose. This was performed using a Daihan Ultrasonic Bath (CREST-ultrasonics) with optimization of ultrasound treatment conditions initially carried out as described in literature [22]. After

the exposure time, treated fibers were thoroughly rinsed in water flow to remove excess alkali. Few drops of very dilute acetic acid solution were added and washing was continued until the waste wash water no longer show traces of alkalinity i.e. pH 7 attained. These fibers were left in air for 24 h after which they were oven dried at 60^{o}C for 8 h. Secondly, PDMS was imparted on to the treated EFB fiber surface to enhance its compatibility with PLA. Treated fibers were soaked in a solution of water and acetone (50:50 by volume) with 1% silane concentration for 2 h [25]. Silane treated fiber were left in air for 8 h to complete the condensation reaction after which they were dried in oven at 60^{0}C for 6 h.

Composites were fabricated from treated EFB fibers and PLA, maintaining the 30 wt% fiber content for all categories of composite. Samples which were prepared for further studies include raw EFB fibers (RF), ultrasound-alkali treated EFB fibers (UAF), ultrasound-alkali silane treated EFB fibers (UASF), pure PLA, raw EFB/PLA composites (RFPC), ultrasound-alkali treated EFB/PLA composites (UAFPC) and ultrasound alkali silane treated EFB/PLA composites (UASFPC).

2.2.3. Fourier Transforms Infrared Spectroscopy (FTIR)

FTIR analysis was carried out to study the bonding structures of untreated and treated EFB fibers and their composites. For this analysis, a Germany Thermo scientific Nicolet 6700 FT-IR spectrometer was used. The analysis was carried out using the standard KBr method, taking wavenumber range from 4000-700 cm^{-1}.

2.2.4. Scanning Electron Microscopy (SEM)

Surface morphologies of untreated and treated EFB fibers were investigated using a scanning electron microscope (ZEISS, EVO 50, Germany). To make samples conductive, they were coated with platinum using a sputter-coater machine, before observing them under the SEM apparatus.

2.2.5. Tensile Testing

Specimens were prepared for tensile testing according to ASTM 638- 08. Testing was performed using a Shimadzu universal tensile machine (model- AG-1), having a 5 KN load cell running at a crosshead speed of 10 mm min^{-1} on tensile samples with 65mm guage length. Seven samples were tested for each composite batch out of which average of five replicate samples was recorded for tensile strength (TS) and tensile modulus (TM).

2.2.6. Flexural Testing

Flexural testing was carried out in line with ASTM D790-97 standard on samples with dimensions of 125 mm x 3.3 mm x 12 mm using a Shimadzu universal tensile machine (model- AG-1) with static load cell of 5 KN. The machine was operated at a cross head speed of 10 mm min^{-1}, with support kept at 50 mm apart. Average of five replicate samples out of seven tested samples for each composite batch was recorded for flexural strength (FS) and flexural modulus (FM).

2.2.7. X-Ray Diffraction (XRD)

XRD analysis was carried out in order to determine the crystalline structure of composites, arrangement of atoms within the composite, crystallite size and likely imperfections. Analysis was performed at a scanning speed of 1deg min^{-1}, sampling step of 0.02^o, scanning range 3-30^o at a wavelength of 0.541 nm using an XRD goniometer. Some of the important parameters to be noted is the interplaner spacing [d(Å)] of the planes in the crystals. The interplaner spacing is related to the Bragg scattering angle (θ) and X-ray wavelength (λ), by:

$$d = \frac{\lambda}{2sin\theta} \quad \text{……...……..} \quad (1)$$

Where, d = interplaner spacing, θ = Bragg angle and λ = X-ray wavelength.

On the other hand, the crystallite size gives further information about the strains developed in the crystallites as a result of changes in lattice plains brought about by fiber treatment. This lattice changes are responsible for line shifting in the X-ray diffractogram. Crystal size, which is a measure of the size of coherently diffracting domain can be gotten using the Scherer's equation [26].

$$Crystallite\,Size = \frac{K\lambda}{\beta cos\theta} \quad \text{……..…} \quad (2)$$

Where, λ = X-ray wavelength, θ = diffraction angle, K = Scherer's constant (0.94) and β = full width at half maximum (FWHM).

To obtain the crystallite size in nanometer, the factor 57.3 was used to convert the value of β from degree to radians. Crystallinity index (CrI%) of the material was gotten according to Segal empirical method [26].

$$CrI\% = \left(\frac{I_{002} - I_{am}}{I_{002}} \right) x100 \quad \text{.....} \quad (3)$$

Where, I_{002} is the maximum intensity of the *002* lattice reflection of cellulose crystallographic form (I) at $2\theta \approx 22.5^{o}$ and I_{am} is the intensity of diffraction of the amorphous material at $2\theta \approx 16.2^{o}$.

2.2.8. Contact Angle

Wettability of the fibers and EFB/PLA composites was measured by a contact angle meter (Goniometer). For fibers, the transgenic falling method was used to analyse the captured video images of water droplets hanging on to the horizontally immersed fiber. For composites, 5 µl of water droplet was allowed to rest on the specimen and images were captured. Fifteen images were analysed for each sample with the help of contact angle software (model- JY-82), and average of ten images result were computed to obtain the contact angle.

2.2.9. Differential Scanning Calorimetry (DSC)

A DSC instrument (model: TA/Q-1000) was used to determine the glass transition temperature (T_g), crystallization temperature (T_c) and melting temperature (T_m) of the composites. A heat/cool/heat method was used with a range of temperature from 30 to 250^{o}C at a heating and cooling rate of 10 and 5^{o}C min^{-1}, respectively. Nearly 3 to 5 mg of each sample was considered for the experiment.

2.2.10. Thermogravimetric Analysis (TGA)

TGA was carried out using a TA analyser (TGA Q500 V6.4, Germany). Nearly 5 mg of each sample was placed in a platinum crucible under nitrogen atmosphere at a flow rate of 40 mL min^{-1}. Samples were heated at 20^{o}C min^{-1} in the range from 25-600^{o}C.

3 RESULTS AND DISCUSSION

3.1 Properties Of Fiber

3.1.1 FTIR Analysis

The FTIR spectra for RF, UAF, and UASF fiber are illustrated in Figure 1. On a general note for all the fiber types, the conspicuous peaks include the broad peak from 3200-3600 cm^{-1} which is a characteristic peak from vibrations of the stretching of hydrogen bonded –OH groups. For RF, the peak at 2924 cm^{-1} represents stretching vibrations from C─H groups of the cellulose and hemicellulose components of EFB fibers. The peak at 1727 cm^{-1} is due to C=O stretching of ester and carboxylic components of EFB hemicellulose and lignin. The peaks at 1644 cm^{-1} and 1514 cm^{-1} are characteristics of =CH vibrations from aromatic skeletal and –C=C bending in lignin components of the fiber respectively. The peak at 1422 cm^{-1} represents $–CH_3$ asymmetric and C─H symmetric deformation of fiber lignin. Representations of the C=H stretching in methyl, methylene and methoxy groups of lignin was noticed at 1318 cm^{-1}, whereas aromatic C─H in-plane deformation of lignin is evident at 1034 cm^{-1}. The peak at 1241 cm^{-1} represents asymmetric stretching of –C-O-C- in the β-glycosidic bond of cellulose chain.

On the other hand, UAF fibers showed similarity in peaks with RF fibers. The major differences are the weakening and sharpening of peaks at certain points, as well the

disappearance of peaks at some other point. Conspicuous among these is the disappearance of the peak at 1727 cm^{-1} for RF. This suggests an effective removal of significant portions of the fiber hemicellulose and lignin due to ultrasound and alkali treatment of EFB fibers, as reported elsewhere [22]. Also the peaks at 1644cm^{-1} for RF was found to appear at a lower wavelength for UAF fiber, indicating some structural changes to the fiber after treatment with ultrasound and alkali. Structural changes to fibers with respect to fiber treatment were also reported by other researchers [25, 27]. Other noticeable changes to the spectrum of UAF fiber include the reduction in absorption intensity as well as little upward shifting of the peak at 1422 cm^{-1}, which indicates partial removal of hemicellulose and lignin from fibers as reported elsewhere [19]. The sharpness of the peak at 1318 cm^{-1} for the case of UAF fibers, further confirms the effective removal of hemicellulose and lignin from EFB fiber after ultrasound and alkali treatment [22].

The spectrum for UASF fibers also reveals some important peaks which include at 902 cm^{-1}, which had been reported to represent Si-O asymmetric stretching in Si-O-Si or cellulose-O-Si bonds [28]. This peak could be associated to some condensation reactions between the hydrolysed silane and cellulose hydroxyl groups of EFB fiber after treatment with silane coupling agent (PDMS). Condensation reactions between fiber –OH groups and hydrolysed silane have also been reported in a similar research [29]. The peak at 802 cm^{-1} which represents C-Cl stretching in alkyl halide could be from the chlorine terminated silane (PDMS) used for this research. Other peaks observed for UASF are the small peaks around 846 cm^{-1} and 765 cm^{-1} which represents Si-C bonds [30]. The

smallness size of theses peaks could perhaps be as a result of the concentration of silane on EFB fiber surface as reported elsewhere [27].

3.1.2 Surface Morphology

The SEM images of RF, UAF and UASF are shown in Figure 2a, 2b and 2c. The image, Figure 2a, representing untreated EFB fiber (RF) can be seen to possess surface morphology consisting of covered pore spaces. The cementing substances which are usually found on the surface of untreated EFB fibers might range from dirt particle, waxes, pectin, silica bodies and other solubles. On the other hand, the image for UAF (Figure 2b) can be seen to compose of several opened pores. This indicates that treatment with ultrasound in alkali medium had disrupted the surface structure of the fiber. Ultrasound treatment of fibers works via mechanical and thermal energies supplied by ultrasonic cavitation. The mechanical energy helps to disengage the fiber bundle, leading to fibrillation whereas the thermal energy serves to heat up the alkali such that binding structures like lignin and hemicellulose can be dissolved out. As the ultrasound treatment continues in an alkaline medium, there is more possibility for alkaline to penetrate the fiber, thereby opening up the cavities within the fiber in form of pores. On the overall, there is a disruption of the hydrogen bonding in the EFB fiber structural framework, leading to the opened pores as noticed on the surface of UAF fiber. These opened pores are good incentives for better interlocking between fibers and polymer matrix during composite fabrication, as reported elsewhere [22, 25].

Furthermore, SEM image for UASF fiber (Figure 2c) reveals silane coupling agent well planted unto the fiber surface in form of very light and thin films. The exposure of cellulose –OH groups of EFB fibers due to ultrasound and alkaline treatment, gives room for some condensation reactions between the silane and cellulose hydroxyl groups of the EFB fiber. This reaction serves to replace as many hydroxyl groups as possible on the fiber surface, through the formation of cellulose-O-Si bonds [28]. Reduction in number of hydroxyl groups on the fiber surface helps to reduce its hydrophilic tendencies by imparting hydrophobic properties unto the fiber surface, as confirmed by results from EFB water contact angle measurement. The resultant effect of this would be an improved fiber matrix adhesion, and subsequently composites with greater mechanical properties [31, 32].

3.1.3 Wettability

The CA values for RF, UAF and UASF are shown in Table 2. It can be seen that the hydrophilic properties of EFB fibers increased due to ultrasound treatment in alkali medium, making the CA to decrease from 35^{o} for RF to 30^{o} for UAF. This could be as a result of the removal of hydrophobic components like lignin from EFB fibers due to ultrasound treatment in alkali medium [33]. This led to an increased availability of hydroxyl groups on the fiber surface. Exposure of hydroxyl groups on the surface of treated fibers have also been reported elsewhere [34, 35]. Presence of hydroxyl groups on the fiber surface thus increased the wettability of the treated fibers by water, thereby reducing its CA. For silane treated fibers (UASF), the CA can be seen to increase from 30^{o} (UAF) to 46^{o} (UASF)). This notable increase could be associated with the

hydrophobic properties imparted unto the EFB fibers after treatment with silane (PDMS). Initial treatment of EFB fibers with ultrasound and alkali would open up the pores on the fiber surface, as well as exposed the cellulose hydroxyl groups [29], giving enough room for PDMS to be fully engrafted unto the fiber surface. Presence of PDMS on the fiber thus imparts hydrophobic properties unto the fiber, making it less wettable by water hence, an increased CA value. Increased hydrophobicity of treated fiber was also reported by other researchers [28, 31, 32].

3.1.4 Structural Analysis

The X-ray diffractograms for RF, UAF and UASF are illustrated in Figure 3. Two conspicuous peaks were noticed for each fiber type at $2\theta \approx 22.5^{o}$ and $2\theta \approx 16.2^{o}$. These important peaks which represent the crystalline and amorphous components of cellulose respectively were analysed and the data are included in Table 3. The conspicuous crystalline peak for untreated EFB fiber (RF) was noticed around $2\theta = 22.17^{o}$, which represent the crystallographic (002) planes of the cellulose components in EFB fiber [26]. This position was found to shift towards the higher angle after treatment, making the position to be observed at 22.31^{o} (UAF) and 22.47^{o} (UASF). This shifting indicates a decreased interplanar spacing of the (002) planes, suggesting that a closer packing had taken place between the cellulose crystal structures, perhaps due to the removal of hemicellulose, pectin and lignin from EFB through treatment with ultrasound in alkali medium [36]. The reduction in FWHM after treatment as well could be as result of new hydrogen bonding between some of the cellulose chains after treatment making it rearrange and pack more closely [19, 36]. Likewise, the increase in both of crystal size

and crystallinity of UASF over UAF could be due to some transcrystallinity brought about by combined ultrasound, alkali and silane treatment of EFB fibers [19].

3.2 Properties Of Efb/Pla Composites

3.2.1 FTIR Analysis

The FTIR spectra for PLA, RFPC, UAFPC and UASFPC are listed in Table 4. Generally, the spectrum for pure PLA, RFPC, and UAFPC look in many ways similar except for the reduction in peak intensity at some points as well as the shifting of bands at some other points perhaps due to bonding between PLA and EFB fibers. Most of the bonds in pure fiber can be seen to be left as they were perhaps due to esterification reactions between the –OH of EFB fibers and terminal –COOH groups of PLA as reported elsewhere [22].

The major observed peaks are 3500-3200 cm^{-1} which represent –OH stretching, 3050-2850 cm^{-1} which is an attribute of vibrational stretching from C-H of the methyl and methylene moieties of cellulose and hemicellulose. The conspicuous peak at 1750 cm^{-1} represents stretching of the carbonyl (C=O) group of acetyl and carboxylic acids moieties in hemicellulose and lignin, and the ester components from PLA. Presence of C-C asymmetric stretching in aromatic rings was revealed at 1454 cm^{-1}. The symmetric deformation of C-H components was revealed by the band at 1359 cm^{-1}. Stretching of C-O of carboxylic acid and ester components of PLA was revealed around 1128 cm^{-1}. This peak also represents vibrational stretching of both amorphous and crystalline cellulose. The major difference in the spectrum for RFPC and UAFPC is the peak at 1750 cm^{-1} (C=O stretching) from PLA. This peak manifested with a reduced intensity in RFPC due

to reduced bonding between RF and PLA. Presence of hemicellulose and lignin in RF would reduce the number of available –OH groups on the fiber surface for bonding with PLA [19]. However, for UAFPC, there was total disappearance of the peak, which is attributed to fiber treatment that opened up many cellulose –OH groups of the fiber for bonding with C=O groups of PLA [22].

On the other hand, the spectrum for UASFPC seems to be a little different from other composites. Some of the notable peaks include 1755 cm^{-1} and 1715 cm^{-1} which represents C=O stretching in carboxylic acid and ketone. Peak at 1456 cm^{-1} which represents C-H bend in alkanes and 1366 cm^{-1} which represents C-H rock in alkanes are from the methyl components of PDMS, peak at 1091 cm^{-1} represent C-H wag in alkyl halides from the haloform reaction of PDMS with –OH of EFB fiber cellulose. The reactive nucleophilic substitution of the chlorine molecule present in the silane coupling agents used (Chlorine terminated PDMS) by hydroxide from EFB cellulose during the haloform reaction. Vibration around 930-950 cm^{-1} represents stretching of Si-O-Si or cellulose-O-Si bonds formed as a result of the direct condensation reactions between PDMS and –OH of OPEFB fibers [28]. The peak at 864 cm^{-1} and 755 cm^{-1} is attributed to Si-C bond as reported elsewhere [30].

3.2.2 Mechanical Properties

The tensile and flexural properties of EFB fiber reinforced PLA composites are illustrated in Figure 4a and 4b. It can be seen that the tensile strength (TS) and tensile modulus (TM) of pure PLA was found to be 55.9 and 1195 MPa, respectively, which was

increasing up to 30 wt% fiber loading, with observable decreasing trend at 40wt%. The low values of tensile properties at 10 and 20 wt% loading are thought to be due to the inadequate amount of fibers, which may results in ineffective stress transfer and distribution [22]. The highest values for TS and TM were noted as 59.2 and 1571 MPa, respectively, at 30 wt% fiber loading. Thus the improvement of TS was found to be 5%, whereas 31% for TM. The even distribution of fibers within the matrix at 30 wt% loading and the desirable strength of the individual EFB fibers are probably the reasons behind it [19, 22]. At 40 wt% fiber loading the values was found to be decreased to 57.2 and 1498 MPa, respectively. This decrease could be as a result of poor wetting of EFB fiber by the PLA matrix due to excessive fiber loading. Moreover, uneven distribution and agglomeration at higher loading was the negative outcomes [37, 38]. Similar trend was observed for the case of flexural properties. The flexural strength (FS) and flexural modulus of pure PLA was found to be 83.02 and 936 MPa, whereas those of EFB/PLA composite at 30 wt% were found to be 99.18 and 1469 MPa. This is an increase of about 19% and 57% respectively for FS and FM. The decrease in flexural properties at 40 wt% perhaps due to overloading effect of the fiber on the PLA matrix, leading to excessive stress transfer breaks [19].

A graphical comparison of the mechanical properties of PLA, RFPC, UAFPC and UASFPC is drawn in Figure 5a and 5b. The TS of UAFPC and UASFPC were found to be 73.1 and 84.8 MPa, whereas their TM is 2099 and 2671 MPa respectively. Also, the FS was found to be 116 and 129 MPa and FM was found to be 1758 and 2570 MPa, respectively, for UAFPC and UASFPC. From the figures, it is clear that UASFPC shows

the higher tensile and flexural properties than that of UAFPC. The increment in TS, TM, FS, and FM of UASFPC over RFPC are 43, 70, 30 and 75% respectively, whereas for UAFPC over RFPC it is 23.5%, 33.6%, 16.8% and 19.6% respectively. The improved performance of UAFPC and UASFPC can be attributed due to enhanced fiber-matrix interfacial adhesion [22]. The effective delignification of EFB fibers through the cavitation effect of ultrasound treatment in alkali medium is thought to be a reason for good interaction with the matrix [26]. The improved fiber-matrix interfacial adhesion invariably led to effective stress transfer between the PLA matrix and EFB fiber, thus producing composites with improved mechanical properties [38]. The silane treatment was also found to be effective to improve the mechanical properties as an outcome of higher interfacial adhesion [8, 40].

3.2.3 Wettability

The CA of pure PLA and EFB/PLA composites are included in Table 2. It can be seen that CA for RFPC and UAFPC are lower compared to PLA. This could be due to the presence of hydrophilic fibers in the composites. The CA value for UAFPC was found to be higher (89^{o}) compared to that of RFPC (79^{o}). This can be associated with effective fiber treatment, which made interfacial interlocking between fiber and PLA matrix more possible for UAFPC than RFPC. The enhanced surface interaction due to treatment with ultrasound and alkali made the PLA matrix to be properly embedded into the fiber, as well covering and shielding the surface from external factors including water. This would lead to the exposure of less fiber on the surface of UAFPC compared to RFPC, making the wettability of UAFPC more reduced leading to an increased contact angle. Increase in

CA for permanganate treated soy hull has also been reported elsewhere [41]. Whereas reduced exposure of fiber on composite surface after treatment was also noticed by some other researchers [19, 22]. On the other hand, for UASFPC, it can be seen that the CA was higher than for other composites and even for PLA, indicating non-wettability. This could be accrued to the hydrophobic properties of PLA combined with the hydrophobic nature of PDSM, which shields the composite surface from spontaneous wetting by water. This conforms to the findings of some other researchers [41, 42].

3.2.4 XRD Analysis

The X-ray diffractograms of PLA, RFPC, UAFPC and UASFPC are illustrated in Figure 6. From the pattern of the diffractogram, a low degree of crystallinity due to diffused peak at $2\theta = 15.4^{o}$ for PLA can be seen, indicating that PLA chains are not well ordered. A similar peak for injection moulded PLA was observed elsewhere [22]. On the other hand, RFPC, UAFPC and UASFPC showed a less diffused peak with intense peak around $2\theta \approx 22.5^{o}$. Summary of the XRD parameters for PLA, RFPC, UAFPC and UASFPC are included in Table 3. It can be seen that the position of the crystalline peak was shifted to the higher angle after the inclusion of fibers into PLA, perhaps due to macro stress on the PLA matrix after fiber inclusion. This could decrease the average molecular distance of the PLA molecules as well reduce amorphous nature [22], as indicated by the d-spacing values in Table 3. Crystallite size and crystallinity index was found to be maximum for UASFPC, followed by UAFPC. This suggests that ultrasound and alkali treated OPEFB fibers were able to act as nucleating agents for PLA crystallization perhaps due to effective interfacial bonding of the treated fibers with PLA

[39, 40]. This might have served to increase the tendency for transcrystallinity within the composite as reported elsewhere [19]. Furthermore, the reduction in FWHM indicates higher crystallinity, as well as the sharper peak as seen from the X-ray diffractogram of treated fiber composites. For the case of RFPC, the low improvements observed for crystallite size and crystallinity index could be because the untreated EFB fibers were too large to effectively restrict the mobilization of macromolecular molecules in the polymer chain of PLA matrix, similar to findings of other researchers [43, 45]. It could as well be that the untreated EFB fibers could not effectively serve as nucleating agent due to the reduction in number of exposed crystalline cellulose on the untreated OPEFB fiber surface.

3.2.7 Thermal Properties

The DSC thermograms for PLA, RFPC, UAFPC and UASFPC are illustrated in Figure 7. The thermograms reveals three successively distinct transition stages: the first is an endothermic transition which represents the glass transition temperature (T_g), the second is an exothermic transition represents the cold crystallization temperature (T_c) whereas the third which is an endothermic transition represents the melting temperature (T_m) respectively. It can be seen that T_g for all the composite categories are less than for pure PLA. This suggests that EFB fiber was able to provide steric effect that might have inhibited the PLA chain from close packing. This could lead to increase in the free volume of the PLA matrix thereby reducing the T_g as reported in previous research [46]. Reduction in free volume of PLA could be attributed to likely crosslinking through hydrogen bond between the fiber cellulose hydroxyl groups and the carbonyl groups of

PLA [46]. Likewise, the cold crystallization exotherm, $T_{c,}$ for all the composite types can be seen to be shifted to lower temperature than pure PLA. This indicates a speedy crystallization brought about by the presence of OPEFB fibers in the composite which might have acted as nucleating agents for PLA. Similar observations were also reported elsewhere [47, 48], and reasons for this had been attributed to the effect of heterogeneous nucleation which cellulose fibers are capable of inducing into PLA matrix [47].

The endotherm melting peak which represents the fusion the PLA crystallites can be seen around 157-158^{o}C for PLA and the composite samples. Crystallization index of PLA was found to increase due to the incorporation of EFB fibers, and this suggests that there were more crystallites formed due to the activity of EFB fibers which might have acted as nucleating agents that initiated the germination as well as enhance the growth of spherolites as reported elsewhere. Similar observation was recorded in previous research [48], and this also conforms to the result from the XRD analysis. The increase in PLA crystallization for the composites follows UASFPC>UAFPC>RFPC. Increase in crystallization with fiber treatment could be attributed to the creation of more nucleating sites on the fiber surface due to combined effect of ultrasound and alkali treatment which opened up more cellulose hydroxyl groups on the fiber surface. This could speedy initiate the germination and growth of spherolites. Notable however is the high increases for UASFPC perhaps due to better fiber-matrix interfacial adhesion brought about by ultrasound and alkaline treatment followed by coupling effect of the silane coupling agent (PDMS). This could have favoured transcrystallinity within the treated fiber based

composite material as reported by other researchers [19]. Summary of T_g, T_c, and T_m are included in Table 5.

The TGA and DTG curves for PLA, RFPC, UAFPC and UASFPC are illustrated in Figure 8a and 8b. From the curve in Figure 8a, it can be seen that the thermal degradation of pure PLA was in a single stage, with conspicuous onset of weight-loss occurring at 320-385^{o}C. For other composites containing EFB fiber, the degradation can be seen to commence at a lower temperature compared to PLA. The initial drop was observed around 105^{o}C, perhaps due to the release of absorbed moisture. Also, there is a clear distinction between the sharp drop which took place around 290^{o}C for composites and that of pure PLA. Two temperature ranges of 285-385^{o}C and 385-490^{o}C were observed for the composites which may be attributed to the thermal decomposition behaviour of the differently treated EFB fiber molecules in the composites. Although the degradation temperature (T_d) can be obtained from the DTG data plotted in Figure 8b, it is a usual practice to consider the degradation temperature of a sample at 50% weight loss as a pointer for the structural destabilization [26]. The T_d values evaluated for PLA, RFPC, UAFPC and UASFPC are included in Table 5.

3.2.8 Surface Properties

The SEM image of the fractured surface of PLA, RFPC, UAFPC and UASFPC is illustrated in Figure 9. The surface of PLA was found to be smooth as it fractured suddenly during the testing like other brittle polymer. On the other hand, the fiber pull out was apparent and bonding was found to be poor with the polymer matrix for the case

of RFPC. For UAFPC, relatively short length fiber pull out was observed, whereas UASFPC showed very short fiber into the matrix. The better adhesion due to ultrasound and silane was found to be observed for the case of UASFPC. This is probably due to the removal of lignin and other surface impurities, which helps to enhance the interaction and interfacial adhesion between fibers and polymer matix [19].

CONCLUSSION

Composites were fabricated successfully through extrusion and injection molding from EFB fibers and PLA by varying fiber content from 10 to 40 wt%. Fiber loading was optimized by the performances of the composites, and 30 wt% was found to be optimum. Fibers were treated with ultrasound and silane to improve the interfacial adhesion between fibers and matrix. The treatment effects were investigated by evaluating the mechanical, structural, morphological and physical properties of the composites. The best performance was showed by UASFPC with an increment of TS, TM, FS and FM, respectively, of 43, 70, 30, and 75% over RFPC. The crystallinity of PLA was found to be improved due to the inclusion of EFB fibers. In addition, silane treatment of fibers enhanced the crystallinity by 92% compared to PLA as depicted from the XRD analyses. Finally, the hydrophobicity of UASFPC was found to be improved that that of the others through contact angle measurement.

ACKNOWLEDGEMENT

The authors would like to appreciate the Malaysia Ministry of Education for providing financial support for this study under the research grant FRGS (RDU120106), and University Malaysia Pahang for PGRS (GRS140343).

REFERENCES

1. X. Li, L.G. Tabil, and S. Panigrahi, *J. Polym. Environ.,* 15, 25 (2007).

2. M.R. Islam, M.D.H. Beg and A. Gupta. *Bioresour*., 8 3753 (2013).

3. M.N.K. Chowdhury, M.D.H. Beg, M.R. Khan, M.F. Mina and A.F. Ismail, *Colloid Polym Sci*, (2014) DOI 10.1007/s00396-014-3462-y.

M.N.K. Chowdhury, M.D.H. Beg, M.R. Khan, M.F.Mina, *Mater. Letter*., 98 26 (2013).

4. M. Sain and S. Panthapulakkal, *Ind. Crop. Prod.* 23, 1(2006).

5. P. Wambua, J. Ivens, and I. Verpoest, *Compos. Sci. Technol.* 63, 1259 (2003).

6. R. Ramli, M.R. Khan, M.N.K. Chowdhury, M.D.H. Beg, R.M. Halim, A.A. Aziz, Z. Ibrahim, N.H. Zainal, *Advanc. Nanopartic*, 2, 358 (2013).

7. M.N.K. Chowdhury, M.D.H. Beg, M.R. Khan, *Polym. Bull.* (2013) 70 3103 (2013).

8. L. Petersson, I. Kvien, and K. Oksman, *Compos. Sci. Technol.* 67, 2535 (2007).

9. M.S. Huda, L.T. Drzal, A.K. Mohanty, and M. Misra, *Compos. Sci. Technol* 68, 424 (2008).

10. S. Mohanty, S.K. Verma, S.K. Nayak, and S.S. Tripathy, *J. Appl. Polym. Sci.* 94, 1336 (2004).

11. A.K.M.M. Alam, M.F. Mina, M.D.H. Beg, A.A. Mamun, A.K. Bledzki, and Q T.H. Shubhra, *Fibers Polym.*, 15 1303 (2014).

12. R. Bouza, A. Lasagabaster, M.J. Abad, and L. Barral, *J. Appl. Polym. Sci.* 109, 1197 (2008).

13. S. Maiti, R. Subbarao, and M. Ibrahim, *J. Appl. Polym. Sci.* 91, 644 (2004).

14. A. Mohanty, M. Misra, and L. Drzal, *Compos. Interf.* 8, 313 (2001).

15. M. Sreekala, M. Kumaran, S. Joseph, M. Jacob, and S. Thomas, *Appl. Compos. Mater.* 7, 295 (2000).

16. K. Joseph, L. Mattoso, R. Toledo, S. Thomas, L. De Carvalho, L. Pothen, *Natural polymers and agrofibers composites,* vol. 159, 2000.

17. B. Wang, S. Panigrahi, L. Tabil, and W. Crerar, *J. Reinf. Plast. Compos.* 26, 447 (2007).

18. M.R. Islam, M.D.H. Beg, A. Gupta, and M. Mina, *J. Appl. Polym. Sci.* 128, 2847 (2013).

19. Y.T. Didenko, W.B. McNamara, K.S. Suslick, *J. Am. Chem. Soc.* 121, 5817 (1999).

20. A. Valadez-Gonzalez, J. Cervantes-Uc, R. Olayo, and P. Herrera-Franco, *Compos. Part B: Engg,* 30, 309 (1999).

21. A.K.M. Alam, M.D.H Beg, D.R. Prasad, M. Khan, and M. Mina, *Compos. Part A: Appl. Sci. Manuf.* 43,1921 (2012).

22. M.F. Mina, M.D.H. Beg, M.R. Islam, A. Nizam, A.K.M.M. Alam and R.M. Yunus, *Polym. Eng. Sci.* 54, 317 (2014).

23. K. Oksman, M. Skrifvars, and J.-F. Selin, *Compos. Sci. Technol.* 63, 1317 (2003).

24. B.K. Goriparthi, K. Suman, and N. Mohan Rao, *Compos. Part A: Appl. Sci. Manuf.* 43, 1800 (2012).

25. M.N.K. Chowdhury, M.D.H Beg, M. R. Khan, and M. Mina, *Cellulose*, 20, 1477 (2013).

26. N. Sgriccia, M. Hawley, and M. Misra, *Compos. Part A: Appl. Sci. Manuf.* 39, 1632 (2008).

27. M.A. Khan, M.M. Hassan, R. Taslima, and A. Mustafa, *J. Appl. Polym. Sci.* 100, 4361 (2006).

28. C. Hong, I. Hwang, N. Kim, D. Park, B. Hwang, and C. Nah, *J. Indus. Engg. Che.* 14, 71 (2008).

29. M.A. Khan and L.T. Drzal, *J. Adhesion Sci. Technol.* 18, 381 (2004).

30. M.A. Sawpan, K.L. Pickering, and A. Fernyhough, *Compos. Part A: Appl. Sci. Manuf.* 42, 888 (2011).

31. M.A. Sawpan, K.L. Pickering, and A. Fernyhough, *Compos. Part A: Appl. Sci. Manuf.* 42, 310 (2011).

32. M. Khalid, A. Salmiaton, T. Chuah, C. Ratnam, and S.T. Choong, *Compos. Interf.* 15, 251 (2008).

33. S. Suradi, R. Yunus, and M.D.H Beg, *J. Compos. Mater.* 45, 1853 (2011).

34. M. Farsi, "Thermoplastic matrix reinforced with natural fibers: a study on interfacial behavior," *Some critical issues for injection molding," J. Wang (Eds),* pp. 225-250, 2012.

35. C.M. Müller, J.B. Laurindo, and F. Yamashita, *Carbohydrate Polym.* 77, 293 (2009).

36. M. Jacob, S. Thomas, and K. Varughese, *J. Appl. Polym. Sci.* 93, 2305 (2004).

37. S. Joseph, K. Joseph, and S. Thomas, *Inter. J. Polym. Mater.* 55, 925 (2006).

38. S. Ochi, *Mechanics of materials*, 40, 446 (2008).

39. K. Jarukumjorn and N. Suppakarn, *Compos. Part B: Engg*, 40, 623 (2009).

40. B.E. Guettler, C. Moresoli, and L.C. Simon, *Indus. Crop. Prod.* 50, 219 (2013).

41. D. Pasquini, M.N. Belgacem, A. Gandini, and A.A. d. S. Curvelo, *J. Colloid Interf. Sci.* 295, 79 (2006).

42. B.H. Lee, H.S. Kim, S. Lee, H.J. Kim, and J.R. Dorgan, *Compos. Sci. Technol.* 69, 2573 (2009).

43. K.L. Pickering, Y. Li, R.L. Farrell, and M. Lay, *J. Biobased Mater. Bioenergy*, 1, 109 (2007).

44. A. Awal, S. Ghosh, and M. Sain, *J. Therm. Analysis calorimetry*, 99, 695 (2010).

45. P. Krishnamachari, J. Zhang, J. Lou, J. Yan, and L. Uitenham, *Inter. J. Polym. Analysis Characteriz.* 14, 336 (2009).

46. A.N. Frone, S. Berlioz, J.F. Chailan, and D.M. Panaitescu, *Carbohyd. Polym.* 91, 377 (2013).

47. F. Arrakhiz, M. El Achaby, M. Malha, M. Bensalah, O. Fassi-Fehri, R. Bouhfid, *Mater. Desig.* 43, 200 (2013).

Table 1. Operation parameters for Extrusion moulding (EM) and Injection moulding (IM) of EFB and PLA composites

EM Conditions		IM Conditions	
Temperature Profile:		Temperature Profile:	
Zone	Temp.	Section	Temp.
Feeding zone:	110^{o}C	Feeding section:	160^{o}C
Mixing zone:	175-185^{o}C	Compression section:	175-185^{o}C
Metering zone:	190^{o}C	Metering section:	190^{o}C
Die:	185^{o}C	Nozzle:	180-185^{o}C
		Mould:	25-30^{o}C
Screw speed:	100-110 rpm	Screw speed:	155 rpm
Torque:	55-60 (%)	Screw position:	28.5 mm
		Injection time:	0.45 sec
		Cooling time:	25 sec

Table 2. Contact angles of different fibers and composites

Samples	Contact angle (^{o})	Standard deviation
RF	35	0.71
UAF	29	1.09
UASF	47	2.32
PLA	94	1.96
RFPC	79	3.05
UAFPC	89	3.11
UASFPC	106	3.34

Table 3. XRD parameters for different fibers and composites

Samples	Peak position (2θ)	FWHM (2θ)	d (Å)	Crystallite size (nm)	CrI (%)
RF	22.17	3.19	4.01	26.50	40.27
UAF	22.31	2.86	3.98	29.60	42.02
UASF	22.47	2.63	3.95	32.20	44.17
PLA	21.20	4.20	4.19	20.00	41.23
RFPC	22.22	3.87	3.99	21.90	44.59
UAFPC	22.34	2.96	3.97	28.60	63.44
UASFPC	22.68	2.54	3.92	33.30	75.44

Table 4. Summary of FTIR spectra for PLA and EFB/PLA composites

Position of bands (cm^{-1})	Functional group representation
3500-3200	-OH stretching (H-bonded)
3050-2850	C-H stretching vibrations of cellulose and hemicellulose
1750	C=O stretching of hemicellulose and lignin
1454	C-C asymmetric stretching in aromatic rings
1359	C-H symmetric deformation in lignin
1128	C-O stretching of carboxylic acid and ester
UASFPC	
1755	C=O stretching of carboxylic acids and ketones
958, 939	Si-O asymmetric stretching
864 cm^{-1}, 755	Si-C bond

Table 5. Thermal properties of PLA and different composites.

Samples	T_g (^{0}C)	T_c (^{0}C)	T_m (^{0}C)	T_d (^{0}C)
PLA	63.52	116.03	157.39	364
RFPC	61.04	101.32	157.67	322
UAFPC	61.14	102.08	158.04	340
UASFPC	60.90	102.79	158.59	344

Figure 1. FTIR spectra of raw and treated EFB fibers.

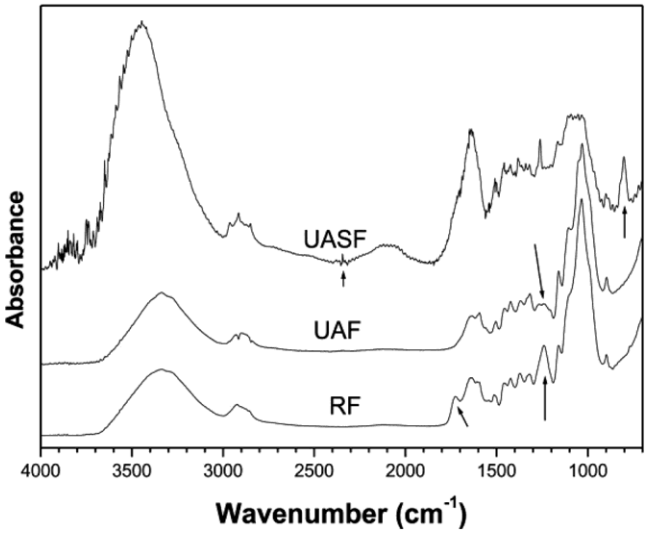

Figure 2. SEM images of raw (a), ultrasound treated (b) and ultrasound-silane treated (c) EFB fiber.

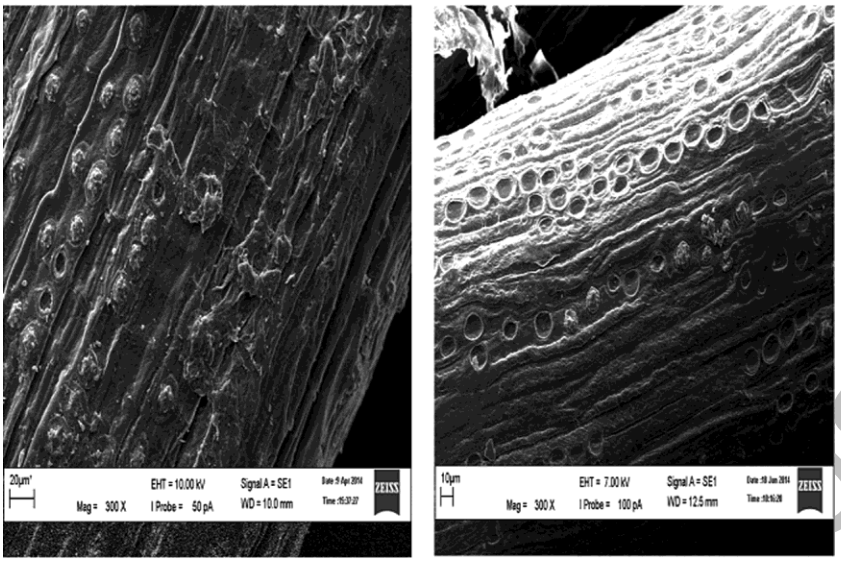

(a) (b)

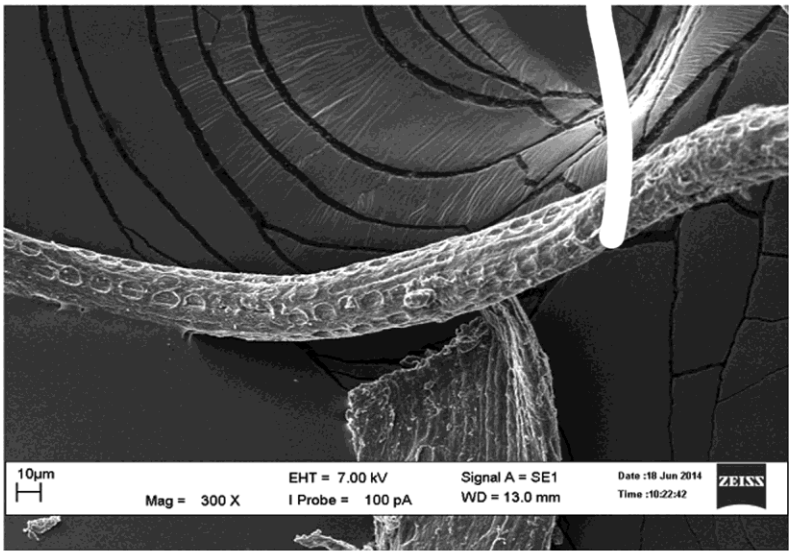

(c)

Figure 3. XRD diffractograms of untreated and treated EFB fibers.

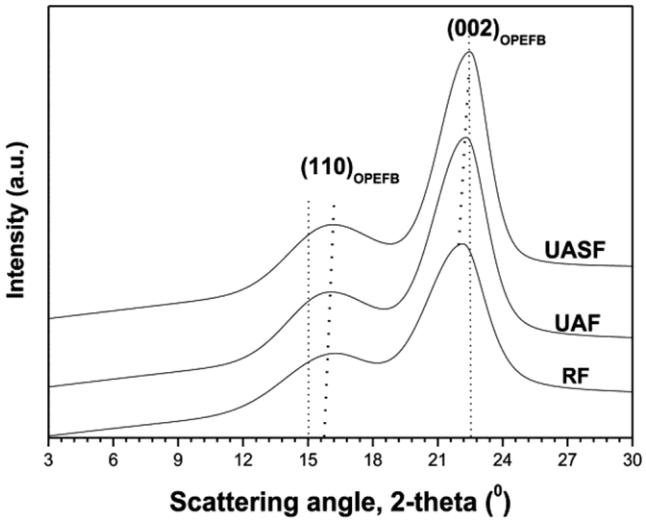

Figure 4. Tensile (a) and flexural (b) properties of pure PLA and composites.

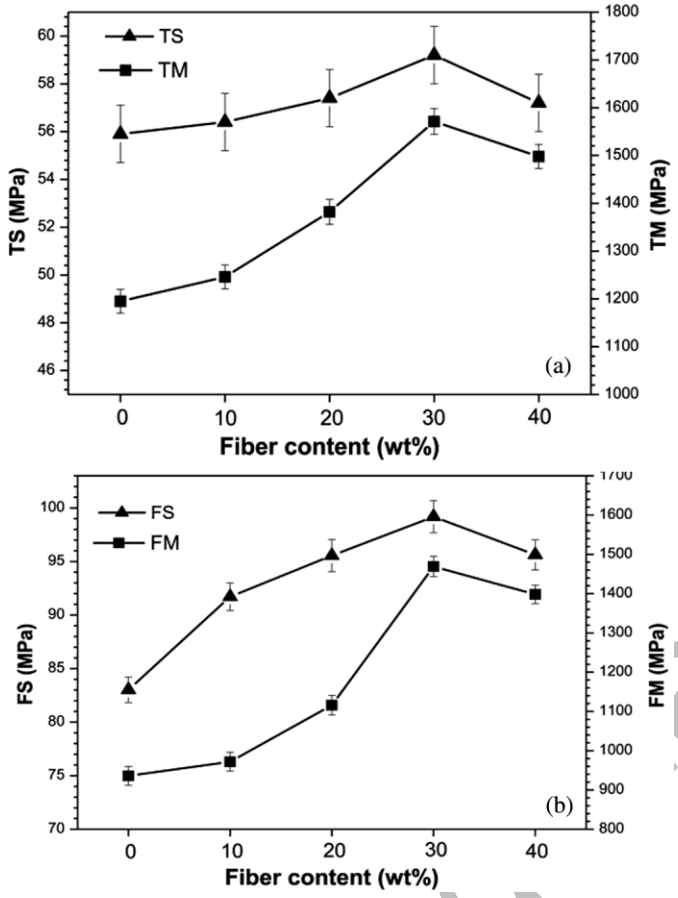

Figure 5. Tensile (a) and flexural (b) properties of pure PLA, RFPC, UAFPC and UASFPC.

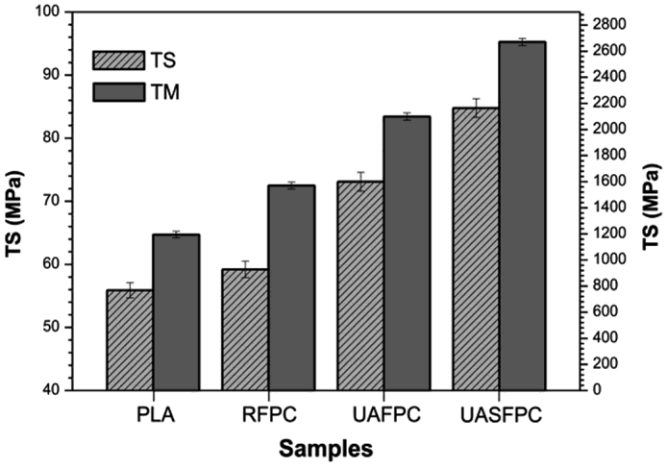

(a)

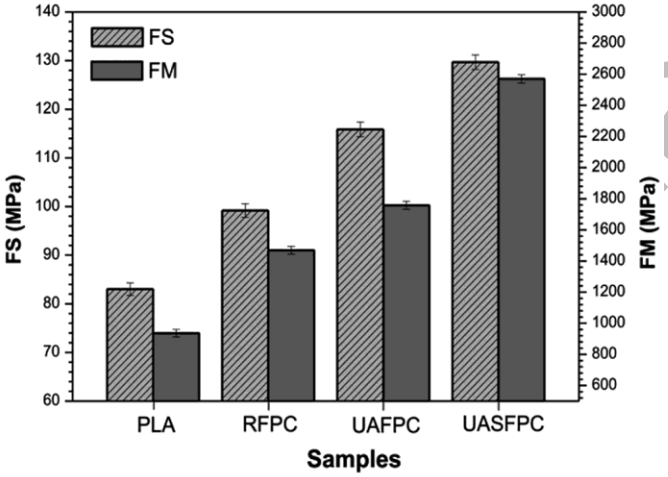

(b)

Figure 6. XRD diffractograms for PLA, RFPC, UAFPC and UASFPC.

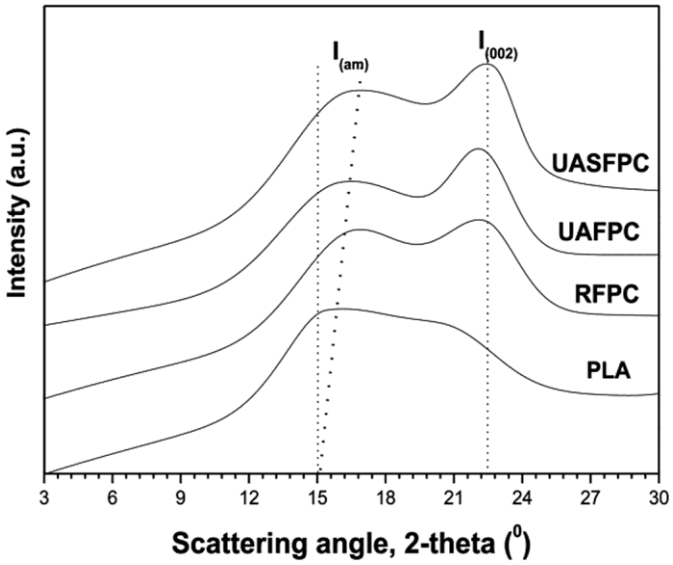

Figure 7. DSC thermograms for PLA, RFPC, UAFPC and UASFPC.

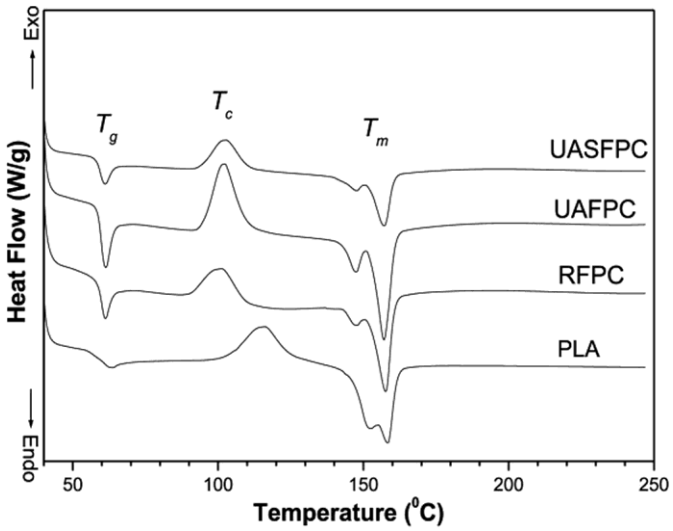

Figure 8. (a) TGA and (b) DTG diffractogram for PLA, RFPC, UAFPC and UASFPC.

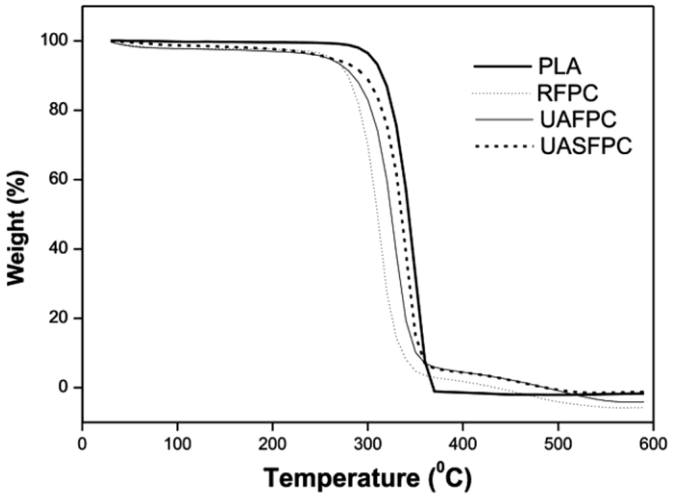

(a)

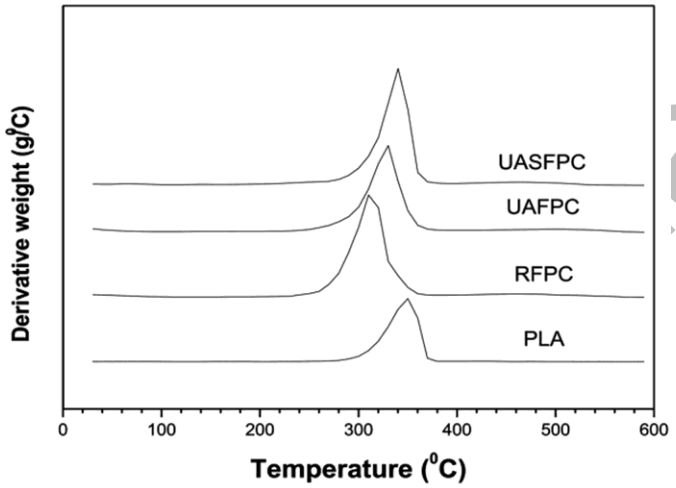

(b)

Figure 9. SEM images of different composites: (a) PLA, (b) RFPC, (c) UAFPC and (d) UASFPC